Clinical Cancer Research

Mobilization of CD8$^+$ T Cells via CXCR4 Blockade Facilitates PD-1 Checkpoint Therapy in Human Pancreatic Cancer

Yongwoo David Seo[1], Xiuyun Jiang[1], Kevin M. Sullivan[1], Florencia G. Jalikis[2], Kimberly S. Smythe[3], Arezou Abbasi[1], Marissa Vignali[4], James O. Park[1], Sara K. Daniel[1], Seth M. Pollack[3], Teresa S. Kim[1], Raymond Yeung[1], Ian Nicholas Crispe[2], Robert H. Pierce[3], Harlan Robins[3,4], and Venu G. Pillarisetty[1]

Abstract

Purpose: Pancreatic ductal adenocarcinoma (PDA) is rarely cured, and single-agent immune checkpoint inhibition has not demonstrated clinical benefit despite the presence of large numbers of CD8$^+$ T cells. We hypothesized that tumor-infiltrating CD8$^+$ T cells harbor latent antitumor activity that can be reactivated using combination immunotherapy.

Experimental Design: Preserved human PDA specimens were analyzed using multiplex IHC (mIHC) and T-cell receptor (TCR) sequencing. Fresh tumor was treated in organotypic slice culture to test the effects of combination PD-1 and CXCR4 blockade. Slices were analyzed using IHC, flow cytometry, and live fluorescent microscopy to assess tumor kill, in addition to T-cell expansion and mobilization.

Results: mIHC demonstrated fewer CD8$^+$ T cells in juxtatumoral stroma containing carcinoma cells than in stroma devoid of them. Using TCR sequencing, we found clonal expansion in each tumor; high-frequency clones had multiple DNA rearrangements coding for the same amino acid binding sequence, which suggests response to common tumor antigens. Treatment of fresh human PDA slices with combination PD-1 and CXCR4 blockade led to increased tumor cell death concomitant with lymphocyte expansion. Live microscopy after combination therapy demonstrated CD8$^+$ T-cell migration into the juxtatumoral compartment and rapid increase in tumor cell apoptosis.

Conclusions: Endogenous tumor-reactive T cells are present within the human PDA tumor microenvironment and can be reactivated by combined blockade of PD-1 and CXCR4. This provides a new basis for the rational selection of combination immunotherapy for PDA.

See related commentary by Medina and Miller, p. 3747

Introduction

Pancreatic ductal adenocarcinoma (PDA) has proven largely unresponsive to T-cell checkpoint therapy and continues to have an extremely high mortality rate (1–4). On the basis of studies in genetically engineered mouse models, the widely accepted explanation for this lack of clinical efficacy is that there is a paucity of effector T cells (T_{eff}) in the PDA microenvironment (5). Specifically, the dense desmoplastic reaction that surrounds these rapidly growing murine PDA tumors is strongly biased toward immunosuppressive cell types, such as myeloid-derived suppressor cells and regulatory T cells (Treg; refs. 6, 7), and contains few T_{eff}. A recent model of cancer immune set points suggests that, unlike an immune desert with no priming of innate immunity and complete tolerance, or a truly inflamed tumor with varied reactive elements, the human PDA microenvironment is one of immune exclusion, with stromal interactions blocking previously primed immune elements (8).

Despite this picture of the PDA immune microenvironment gleaned from murine models, it has also long been known that the presence and infiltration of CD4$^+$ and CD8$^+$ T cells correlates with improved clinical prognosis in patients with PDA (9, 10). Our previous work demonstrated that, unlike the myeloid-predominant microenvironment of PDA mouse models, human PDA is infiltrated by a complex admixture of immune cells, of which T cells, including both effector memory CD8$^+$ T cells and Treg, are typically the largest component (11). A more recent study has further characterized the dynamic interaction of both T_{eff} and Treg with the desmoplastic components of the human PDA microenvironment, utilizing a multiplex immunofluorescence imaging approach; the findings from that study support our previous work by describing a complex lymphocyte-predominant immune milieu in which desmoplasia does not inhibit T-cell infiltration and proximity of T_{eff} to cancer cells predicts improved survival (12). We therefore postulate that in human PDA the lack of clinically significant responses to current T-cell checkpoint therapy is not due to the absence of an adaptive immune response, but to the complex interplay between antitumor T_{eff} and regulatory components, which ultimately results in attenuation of antitumor activity (13).

[1]Department of Surgery, University of Washington, Seattle, Washington. [2]Department of Pathology, University of Washington, Seattle, Washington. [3]Fred Hutchinson Cancer Research Center, Seattle, Washington. [4]Adaptive Biotechnologies, Seattle, Washington.

Note: Supplementary data for this article are available at Clinical Cancer Research Online (http://clincancerres.aacrjournals.org/).

X. Jiang and K.M. Sullivan contributed equally to this article.

Corresponding Author: Venu G. Pillarisetty, University of Washington, 1959 NE Pacific St., Box 356410, Seattle, WA 98195. Phone: 206-616-4924; Fax: 206-543-8136; E-mail: vgp@uw.edu

Clin Cancer Res 2019;25:3934–45

doi: 10.1158/1078-0432.CCR-19-0081

Translational Relevance

Patients with early-stage pancreatic ductal adenocarcinoma (PDA) are rarely cured despite treatment with surgery, chemotherapy, and radiation therapy. The disease has also resisted attempts at treatment with immune checkpoint blockade drugs. We studied the immune microenvironment of resected human PDA and found that although $CD8^+$ T cells were often present, they were typically localized to the stroma, and not immediately adjacent to cancer cells. However, T cells within PDA tumors did show evidence of antigen-driven T-cell receptor repertoire selection, indicating possible anti-cancer potential. By inhibiting the CXCR4 chemokine receptor, we found these cells were able to migrate from the stroma into cancer cell-rich regions, and that PD-1 blockade was then able to activate cancer cell killing. These outcomes were consistent across a large number of individual patients' cancers, suggesting that combined blockade of the PD-1 and CXCR4/CXCL12 axes holds promise as a potential therapeutic strategy for PDA.

C-X-C chemokine receptor type 4 (CXCR4) is an alpha chemokine receptor that binds stromal-derived factor 1 (SDF-1, otherwise known as CXCL12; ref. 14). Its role in the adaptive immune response was initially studied within the context of HIV infection (15, 16), and its role in hematopoietic stem cell homing to the bone marrow has also been examined and utilized clinically (AMD3100, a small-molecule CXCR4 inhibitor drug, is used as a stem cell mobilizer in patients undergoing bone marrow transplant; refs. 17–19). More recently, the CXCR4–CXCL12 axis has been studied within the context of tumor immunology, as many carcinomas such as lung and breast have been found to express the receptor or the ligand; however, a uniform effect on tumor progression has yet to be elucidated across tumor types (20, 21). Blockade of the CXCR4–CXCL12 axis has been shown to inhibit immunosuppressive elements in murine models of ovarian and hepatocellular carcinoma (22, 23). Furthermore, Feig and colleagues used a murine model of PDA to demonstrate that a combination of CXCR4 and PD-L1 blockade achieved synergistic tumor kill by reducing the inhibitory effects on T-cell chemotaxis of CXCL12-coating carcinoma cells (24). However, the antitumor effects of this therapy have not yet been demonstrated in human tumors.

T-cell receptor (TCR) immunosequencing has recently emerged as a powerful tool to understand T-cell responses within the tumor microenvironment (25). While TCR immunosequencing has been utilized to measure characteristics such as intratumoral heterogeneity in lung adenocarcinoma as it relates to worse clinical outcomes (26), the role of repertoire clonality, which can be interpreted as a measure of the degree of clonal expansion within a sample, remains to be fully defined in PDA (27). Although recent TCR immunosequencing studies of human PDA revealed a highly clonal population of T cells, there were no significant correlations between clonality and the phenotypes of the adaptive immune response (28, 29). While limited clonality could arise from many mechanisms, the most compelling case for selection of specific T cells can be made when there is a diversity of DNA sequences coding for conserved amino acid sequences, which suggest that different T-cell clones are being selected for identical specificity. To our knowledge, this has not yet been reported in the literature in any solid tumor, including PDA.

Here, using a combination of multiplex IHC (mIHC) and TCR deep sequencing, we demonstrate the presence of clonally expanded populations of tumor-reactive $CD8^+$ T cells within the human PDA. These T cells show evidence of convergent evolution against the same putative antigen within the tumor microenvironment. Most notably, we demonstrate using a live tumor slice culture system (30, 31) that combining CXCR4 blockade with PD-1 blockade potentiates $CD8^+$ T-cell–mediated killing in human PDA.

Materials and Methods

Ethics statement

All investigations performed in relation to this article were conducted according to the principles expressed in the Declaration of Helsinki. Formalin-fixed tissue blocks from previously resected tumors in patients who had not undergone neoadjuvant therapy were gathered under a protocol approved by the Cancer Consortium Institutional Review Board (CC-IRB) at the Fred Hutchinson Cancer Research Center; there was a waiver of consent, as the study was considered to be of minimal risk because the tissue and data were collected solely for research purposes. Fresh tumor samples for slice culture were procured from patients undergoing pancreatic resection for pancreatic tumors, and who provided prior written-informed consent under a research protocol approved by a separate CC-IRB–approved protocol.

mIHC

Formalin-fixed, paraffin-embedded (FFPE) tissues were sectioned at 4 μm onto positively charged slides and baked for 1 hour at 60°C. The slides were then dewaxed and stained on a Leica BOND Rx Stainer (Leica) using Leica Bond reagents for dewaxing (Dewax Solution), antigen retrieval and antibody stripping (Epitope Retrieval Solution 2), and rinsing after each step (Bond Wash Solution). A high stringency wash was performed after the secondary and tertiary applications using high-salt TBST solution (0.05 mol/L Tris, 0.3 mol/L NaCl, and 0.1% Tween-20, pH 7.2–7.6). OPAL Polymer HRP Mouse plus Rabbit (PerkinElmer) was used for all secondary applications.

Antigen retrieval and antibody stripping steps were performed at 100°C with all other steps at ambient temperature. Endogenous peroxidase was blocked with 3% H_2O_2 for 8 minutes followed by protein blocking with TCT buffer (0.05 mol/L Tris, 0.15 mol/L NaCl, 0.25% Casein, 0.1% Tween 20, pH 7.6 ± 0.1) for 30 minutes. The first primary antibody (position 1) was applied for 60 minutes followed by the secondary antibody application for 10 minutes and the application of the tertiary TSA-amplification reagent (PerkinElmer OPAL fluor) for 10 minutes. The primary and secondary antibodies were stripped with retrieval solution for 20 minutes before repeating the process with the second primary antibody (position 2) starting with a new application of 3% H_2O_2. The process was repeated until all 6 positions were completed; however, there was no stripping step after the sixth position. Slides were removed from the stainer and stained with Spectral DAPI (PerkinElmer) for 5 minutes, rinsed for 5 minutes, and cover slipped with Prolong Gold Antifade Reagent (Invitrogen/Life Technologies).

Slides were cured for 24 hours at room temperature, then representative images from each slide were acquired on PerkinElmer Vectra 3.0 Automated Imaging System. Images were spectrally unmixed using PerkinElmer inForm Software and exported as multi-image TIFF's for analysis in HALO Software (Indica Labs).

Multi-spectral images were analyzed using cell detection for nuclear staining in the HALO software. Thresholds for antibody positivity were calibrated for each individual slide, and automated cell counting was utilized. Autofluorescence-generated false hematoxylin and eosin (H&E) images were analyzed by an experienced pancreatic histopathologist (F.G. Jalikis) to categorize each area or image into the following compartments: stroma without any carcinoma cells (S), juxtatumoral stroma (S-C), lymphoid tissue without any carcinoma cells (Lym), and lymphoid tissue with adjacent carcinoma cells (Lym-C).

Conversion of mIHC fluorescence quantification to image cytometry

All object data csv files were converted to a file format in which the fluorescent intensities of each marker for each object was multiplied by a factor of 10^6 and turned into integer form in Excel. Each annotation layer, depending on the histopathologic compartment categorized by false H&E as above, was separated into its own csv file prior to processing. The processed csv files were dragged and dropped into FlowJo 10 (BD Biosciences), and the subsequent fcs files were analyzed using the gating strategy as shown in Supplementary Fig. S6.

TCR immunosequencing

Ten curls of FFPE tissue (each 5-μm thick) immediately adjacent to the slide used for the mIHC analysis were sent to Adaptive Biotechnologies for DNA extraction. In addition, slices of various treatment groups from the slice culture experiments were blocked in FFPE first and subsequently 15 curls of FFPE slice tissue were sent for DNA extraction and subsequent immunosequencing. Immunosequencing of the CDR3 regions of human TCRβ chains was performed using the immunoSEQ Assay at Adaptive Biotechnologies. Sequences were collapsed and filtered to identify and quantitate the absolute abundance of each unique TCRβ CDR3 region for further analysis, as described previously (25, 32). T-cell clonality was defined as 1−Pielou evenness, as described previously; only productive (in-frame) rearrangements were included in these analyses. Identification of TCR sequences shared between pairs of samples was performed using the nucleotide sequence of productive templates. TCR sequencing data are publicly available at https://clients.adaptivebiotech.com/pub/seo-2019-clincancerres.

Tumor slice culture

PDA samples were visually inspected in the operating room immediately after resection. After review of the sterile gross specimen with the on-call surgical pathologist, one to three 6-mm punch biopsies were taken from an area of visible tumor, which would not affect the analysis of margins. The tumor core was taken in sterile fashion from the operating room immediately to the laboratory, where it was mounted on a vibratome (Leica Biosystems). Slices (250-μm thick) were cut sequentially and placed on a permeable polytetrafluoroethylene (PTFE) membrane with 0.4-mm pores (Millicell, MilliporeSigma), which was sitting on top of RPMI media without any additional immune-activating factors or cytokines. These slice cultures were then incubated overnight at 37°C; the day following resection, the RPMI media was switched for RPMI media containing either 20 μg/mL of IgG Isotype Control (BD Biosciences), 20 μg/mL anti-PD-1 antibody (BD Biosciences), or 20 μg/mL anti-PD-1 antibody plus 100 μg/mL of AMD3100 (Sigma-Aldrich). These were incubated for 2–6 days at 37°C (detailed overview of slice culture methodology and validation has been published previously; refs. 30, 31).

Slice culture live microscopy

PDA tumor slices were obtained and cultured as described previously. After 2 days in culture following the above treatment, PDA tumor slices were transferred to a 48-well plate with 500 μL of fresh media into which 10 μg/mL Alexa 488 CD8 antibody (Invitrogen) and 10 μg/mL Alexa 647 EpCAM antibody (BioLegend) were added, as well as SR-FLICA reagent as per the manufacturer's instructions (ImmunoChemistry Technologies). The slices were incubated for 3 hours at 37°C and were subsequently stained using 10 mg/mL Hoechst 33342 (ImmunoChemistry Technologies) for 10 minutes. The slices were washed twice with PBS and returned with their original media containing the treatment to an 8-well culture slide (ibidi USA Inc.) for imaging. To maintain as close to tissue culture conditions as possible while imaging was performed, the slices and media were maintained heated to 37°C using a covered stage (PeCon GmbH) while flushing warmed, humidified CO_2 through the enclosure. The slices were then imaged using a Leica SP8X Confocal Microscope (Leica Microsystems) at 20× magnification. For each treated slice, 1 hour of images was collected at 3 different positions of high-powered fields with a z-stack of 20 mm.

In a time-lapse live microscopy experiment of a single slice before and after treatment (Fig. 5E and F; Supplementary Fig. S5C and S5D), on the day following resection and slicing, the tissue slice culture proceeded directly to be stained with Alexa 488 CD8 antibody and Alexa 647 EpCAM antibody as described above. The slice was washed of these antibodies using PBS and transferred to the culture slide in media that also contains SR-FLICA assay, to view the activation of caspases as it occurred during the time images were obtained. The tissue culture was imaged in 4 positions throughout the slice for 1.5 hours in the same conditions on the confocal microscope as described above, and imaging was paused. The slice was then treated with 20 μg/mL anti-PD-1 antibody plus 100 μg/mL of AMD3100 added to the media and imaging again resumed in 4 positions of high-powered fields throughout the slice for 1.5 hours.

Image processing and data analysis were performed on Leica LAS X Software (Leica Microsystems) and Imaris Software (Bitplane USA). The data and images obtained were visualized using a maximum intensity projection of the 20-mm z-stack. Volumetric fluorescence renders (Fig. 5D and E) were created with Imaris using the surface application. The $EpCAM^+$, $CD8^+$, and $SR\text{-}FLICA^+$ cells were counted manually. All cells were counted that were observed throughout the time imaged at each position in each slice.

Slice culture flow cytometry

Tumor slices were cultured as above and treated with various drug conditions. The treated slices were then digested into single-cell suspension using digestion media containing collagenase, hyaluronidase, and DNase, followed by mechanical dissociation using a mesh cell strainer. The cells were then washed with PBS and stained using fluorescently labeled flow cytometric

antibodies for CD45, CD4, CD8, and live/dead marker. The flow analysis was performed on the LSR2 and Symphony Flow Cytometry Machines (BD Biosciences).

Slice culture supernatant cytokine analysis

After treatment with various drug conditions in the slice culture system, 70 μL of the resulting media was aliquoted into a 96-well plate using duplicates or triplicates for each slice when available. These samples were analyzed for quantification of cytokines using a Luminex Assay (Invitrogen) performed by the Immune Monitoring core facility at the Fred Hutchinson Cancer Research Center (Seattle, WA).

Statistical analyses

Comparisons of mIHC readouts of different histologic compartments was performed using a paired Student *t* test; only samples which contained both carcinoma-containing and carcinoma-lacking stroma or lymphoid tissue were compared, to allow for the most accurate measurement of the impact of cancer cell presence. All survival analysis was performed by dividing the patients into 2 halves based around the median value of the tested metric, and statistical analysis was performed using the Mantel-Cox log-rank method. To correlate survival with mIHC data, the image cytometric data for the patients with 2 separate slides was combined prior to correlating with survival. Productive clonality was calculated as 1−Pielou's evenness as described above. The clone overlap between the duplicate pairs of samples for 6 patients was calculated using the ImmunoSeq Platform (Adaptive Biotechnologies); the top 100 most frequent nucleotide rearrangements were tracked across the paired samples to determine the number of overlapping sequences. The Morisita overlap index was used to compare the degree of overlap between paired and not related patient samples; an unpaired Student *t* test was performed to compare these groups. Nucleotide rearrangement convergence to the same amino acid sequence was calculated using the Rearrangement Details tool for all clones within the dataset. Correlations between clonality and mIHC were performed using linear regression. For IHC quantification of cleaved Caspase-3 staining, an unpaired Student *t* test was used in pairwise fashion to compare treatment groups. For comparing the number of SR-FLICA$^+$ EpCAM cells within 20 μm of CD8$^+$ T cells on live imaging, an unpaired Student *t* test was used.

Results

Human pancreatic cancer harbors an immunosuppressive microenvironment that localizes to juxtatumoral stroma

To understand how the heterogeneous phenotype of immune infiltrates changes in geographic relation to the carcinoma cells, we performed mIHC on whole slides of 30 human PDA surgical resection samples from 24 previously untreated patients (Fig. 1A; Supplementary Table S1). Using the autofluorescence-generated false H&E images, the fields of interest were analyzed by an expert pancreatic histopathologist (F.G. Jalikis) to determine the presence or absence of carcinoma cells within contiguous areas of tumor stroma or lymphoid tissue (Fig. 1B and C). Across tumors, there was a wide range of infiltration of CD4$^+$ and CD8$^+$ T cells, as well as macrophages (mean frequency 9.4%, 9.3%, 2.1%, respectively; mean number of cells analyzed per slide = 94,550; Fig. 2A–E; Supplementary Fig. S1A–S1C). Among CD4$^+$ T cells, 18% had a regulatory T-cell phenotype (CD4$^+$FOXP3$^+$ Treg), while 24% of CD8$^+$ T cells expressed the immune checkpoint receptor PD-1 (Fig. 2F and G; Supplementary Fig. S1D and S1E).

To examine how proximity to carcinoma cells influences the local immunophenotype, we performed deeper analysis of the individual tumor compartments. Compared with stroma without any associated tumor cells visible within the same 20× field (abbreviated S), juxtatumoral stroma containing carcinoma cells (S-C) was infiltrated by fewer CD8$^+$ T cells, while having more Treg and macrophages; a similar pattern was seen in the intratumoral lymphoid compartment, which was consistent with our prior results (ref. 33; Fig. 2D–F; Supplementary Fig. S1B, S1C, and S1E). There were no differences seen in overall CD4$^+$ T-cell infiltration between compartments containing carcinoma cells and those devoid of them, whereas CD8$^+$ T cells more often expressed PD-1 in the pure stromal compartment (Fig. 2C and G; Supplementary Fig. S1A and S1D). Overall, these results suggest there is a bias toward immunosuppression in the juxtatumoral stroma most closely abutting carcinoma cells.

Clonally expanded T cells within the PDA microenvironment demonstrate convergent evolution

Given the extent of CD4$^+$ and CD8$^+$ T-cell infiltration identified in human PDA, we next evaluated whether specific clones were expanded within these tumors. We extracted DNA from the same surgical resection human PDA specimens used for mIHC and performed TCR immunosequencing (Fig. 3A). We did, in fact, detect intratumoral clonal expansion, as measured by productive clonality, compared with normal healthy peripheral blood [mean 0.14 [0.03–0.24] vs. 0.05, respectively]. However, intratumoral T-cell clonality did not correlate with overall survival in our cohort (Fig. 3A and B).

As intratumoral heterogeneity has been reported for multiple tumor types (26, 34, 35), we wanted to determine whether there were variations in T-cell clone frequencies within the PDA microenvironment. We therefore performed TCR immunosequencing on 2 geographically distinct regions of 6 individual tumors. This revealed a high degree of nucleotide-level sequence overlap of the most frequent T-cell clones present in the 2 samples from each tumor; as anticipated, there was an absence of detectable sequence overlap among different patients' tumors (Fig. 3C; Supplementary Fig. S2A and S2B). Interestingly, we observed that many of the dominant high-frequency TCRβ nucleotide sequences encoded common amino acid sequences, thus suggesting "convergent evolution" of these independent clones (Fig. 3D and E). In fact, across all 24 human PDA tumors, there was a strong correlation ($P < 0.0001$) between the relative frequency of an amino acid TCR sequence and the number of different nucleotide rearrangements that coded for that same amino acid sequence (Fig. 3F). These findings demonstrate that clonally expanded T cells within the PDA microenvironment are pervasive throughout the tumor and appear to undergo selective pressure driven by common antigens within the microenvironment.

Evaluating specific T-cell subsets, we found a direct correlation between clonality and CD8$^+$ T-cell infiltration, as measured by mIHC (Fig. 3H). Conversely, intratumoral Treg frequency and PD-1 expression on intranodal CD8$^+$ T cells both correlated negatively with clonality, suggesting potential mechanisms of suppression (Fig. 3G and I). Overall, these results depict a complex immune microenvironment, in which clonally expanded T_{eff} with suspected tumor antigen specificity are suppressed by an

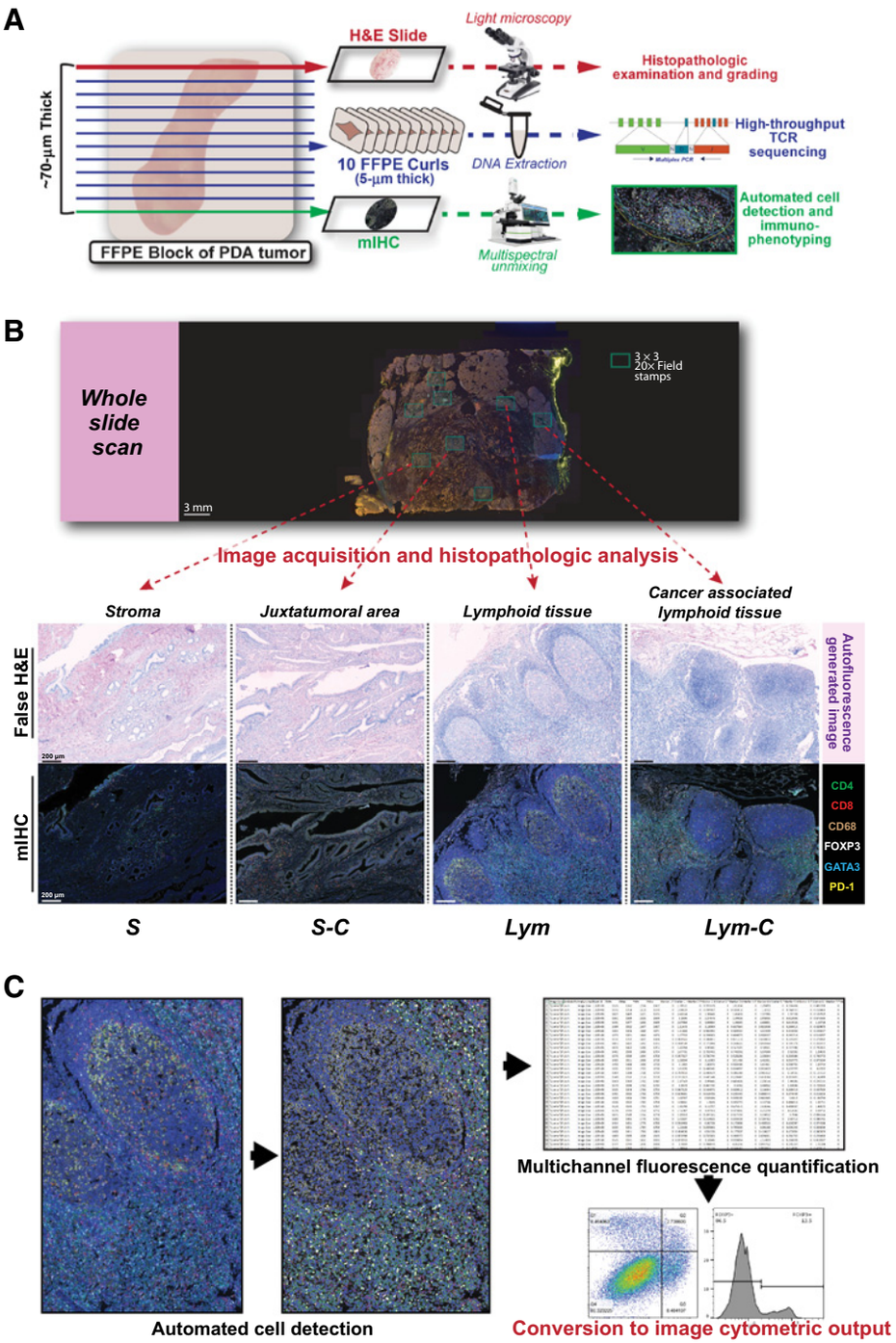

Figure 1.
Multimodal histochemical analysis was performed on human PDA resection samples. **A,** Cutting protocol for FFPE blocks of resection specimens of human PDA from patients who were not treated with neoadjuvant therapy ($n = 30$ from 24 patients). Schema shows layout for performing TCR sequencing and mIHC on adjacent curls of the same block. **B,** Representative whole-slide scan of specimen slide on the Vectra platform were used to evaluate stamps of 3 × 3 20× high-powered fields (shown in both multicolor IHC and matched autofluorescence-generated false H&E images) to differentiate regions containing carcinoma cells and/or lymphoid tissue. **C,** Schema for converting object fluorescence data from mIHC into image cytometric data using FlowJo10.

inhibitory milieu generated by cancer cells and adjacent juxtatumoral stroma.

The immunosuppressive tumor microenvironment can be targeted *ex vivo* to reactivate T cells and generate tumor cell death

Our data analyzing the T-cell immunophenotype and clonotype of resected human PDA suggested that, although there are clonally expanded T cells which appear to be responding to antigens in the tumor microenvironment, the tumor-adjacent/peritumoral stroma exerts a powerful suppressive effect on these T_{eff}. This provides a rationale for the recent failure of T-cell checkpoint therapy in PDA. As previous work using a mouse model of PDA demonstrated that combination therapy blocking the PD-1/PD-L1 and CXCR4/CXCL12 axes had synergistic antitumor effects, we postulated that this combination would similarly reactivate tumor antigen–reactive $CD8^+$ T cells in human PDA.

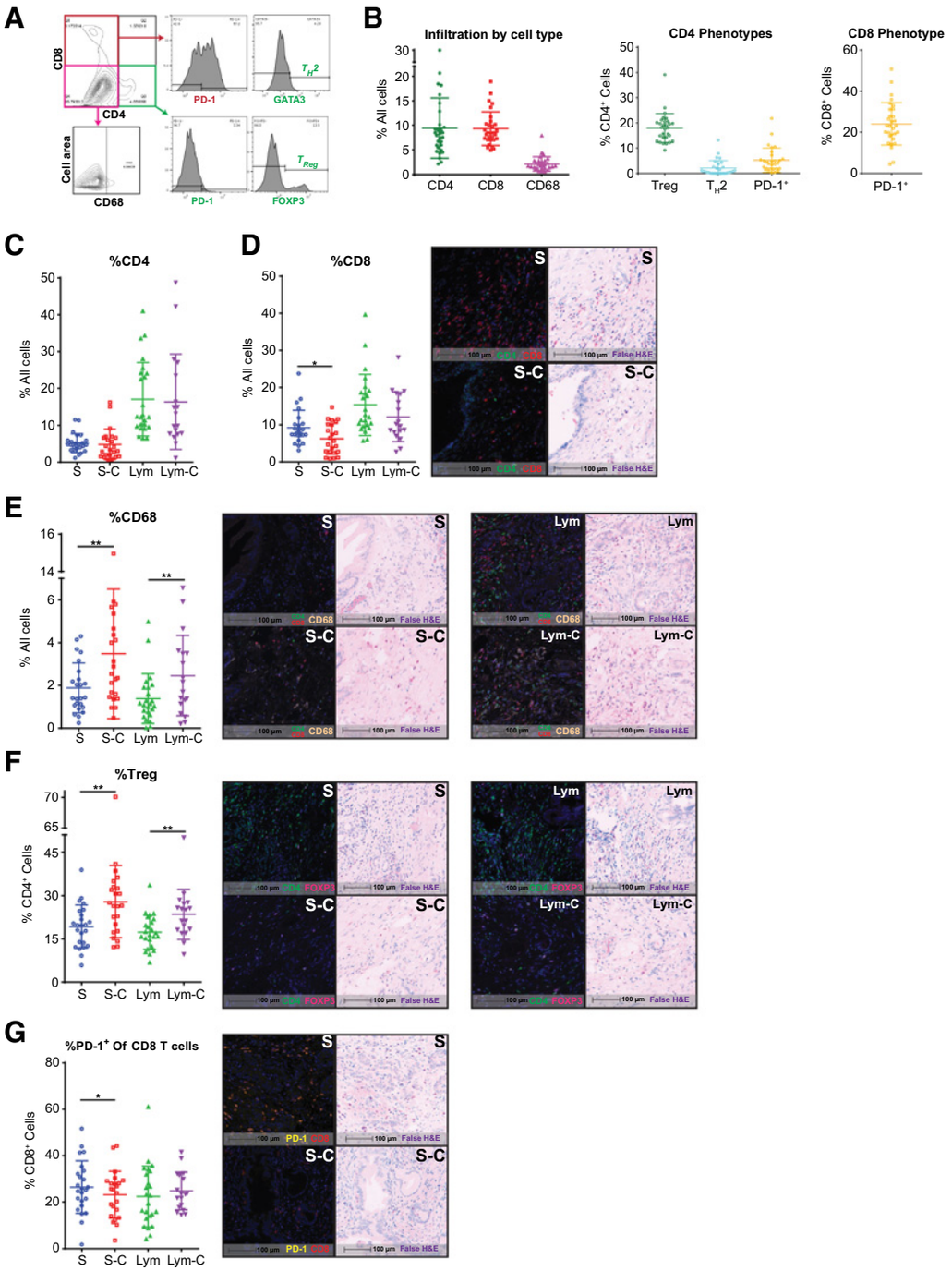

Figure 2.

Juxtatumoral areas contain more immunosuppressive elements. **A,** Representative image for cytometric output and gating strategy. mIHC phenotypes as percentage of all cells analyzed ($n = 30$) within each histologic region [S, stroma; S-C, juxtatumoral stroma; Lym, lymphoid tissue (including lymphoid aggregates or lymph nodes); Lym-C, lymphoid tissue with associated carcinoma cell infiltration]. **B,** Overall T cell and macrophage infiltration throughout entire tumor sections. **C–E,** Tumor containing stroma show lower infiltration of $CD8^+$ T cells and higher infiltration of $CD68^+$ macrophages. Scale bars, 100 μm. Representative multiplex and matched false H&E images are shown for each significant comparison. **F,** Tumor containing stroma and lymphoid tissue have higher Treg infiltration. **G,** PD-1 expression on $CD8^+$ T cells is lower in peritumoral stroma (paired Student *t* tests; *, $P < 0.05$; **, $P < 0.01$).

To interrogate the functional capacity of the resident intratumoral T cells, we utilized our fresh human tumor slice culture platform (Supplementary Fig. S3). We first confirmed by ELISA that CXCL12, the soluble ligand of CXCR4, was detectable within the slice culture supernatant (81–257 pg/mL, $n = 3$, data not shown). We then treated live PDA slice cultures

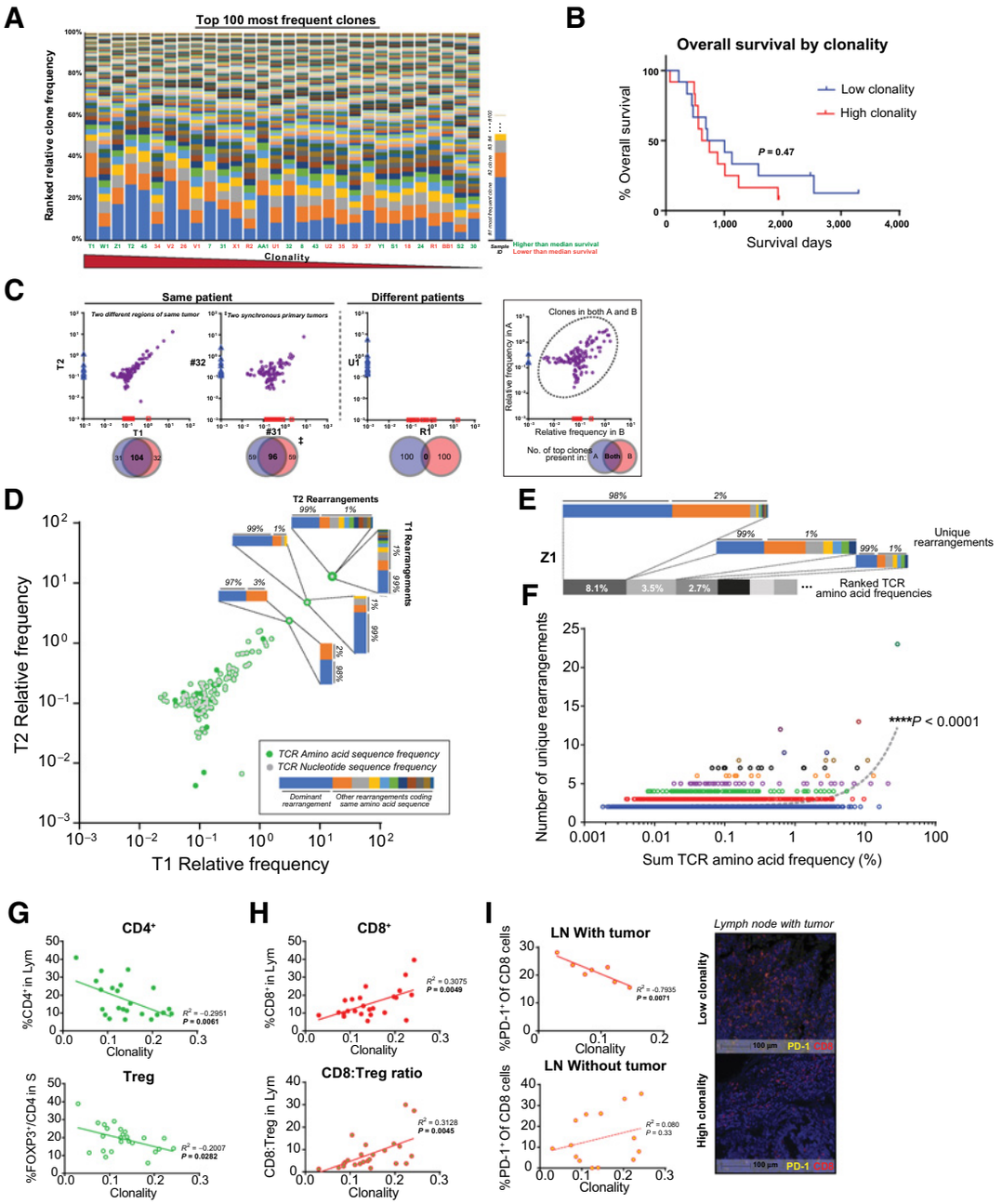

Figure 3.

T cells clonally expand and demonstrate convergent evolution in the PDA tumor microenvironment. **A,** Clonality, as represented by the relative percentage of the 100 most frequent rearrangements within each sample. Arranged in decreasing clonality from left to right. Green sample ID refers to higher than median overall survival; orange is lower than median survival ($n = 30$ samples). **B,** Kaplan–Meier curve between low and high clonality patients, split by median (log-rank test, $n = 24$). **C,** Representative top 100 clone frequency plots of 2 samples from the same patient ($n = 6$ pairs). Each axis represents relative frequency of clone in each sample; purple dots signify clones present in both samples. Venn diagram demonstrates the number of top 100 clones shared. **D** and **E,** Representative plots showing multiple rearrangements code for the same amino acid TCR sequences. Each colored bar represents 1 unique DNA rearrangement. **F,** Positive correlation between the relative frequency of an amino acid TCR sequence and the number of matched DNA rearrangements (linear regression, $n = 30$). Lower %Treg (**G**) and higher %CD8$^+$ T cell (**H**) correlates with higher clonality (linear regression, $n = 23$–24). **I,** PD-1 signal in tumor-positive lymph node (LN) correlate negatively with clonality (representative multiplex image shown; scale bar, 100 μm).

in vitro with a PD-1–blocking mAb, a small-molecule CXCR4 inhibitor (AMD3100), a combination of both drugs, or appropriate controls. There was significantly ($P < 0.0001$) increased necrosis and apoptosis with combined PD-1 and CXCR4 blockade, compared with either monotherapy or control, as evidenced by histology and cleaved Caspase-3 immunostaining

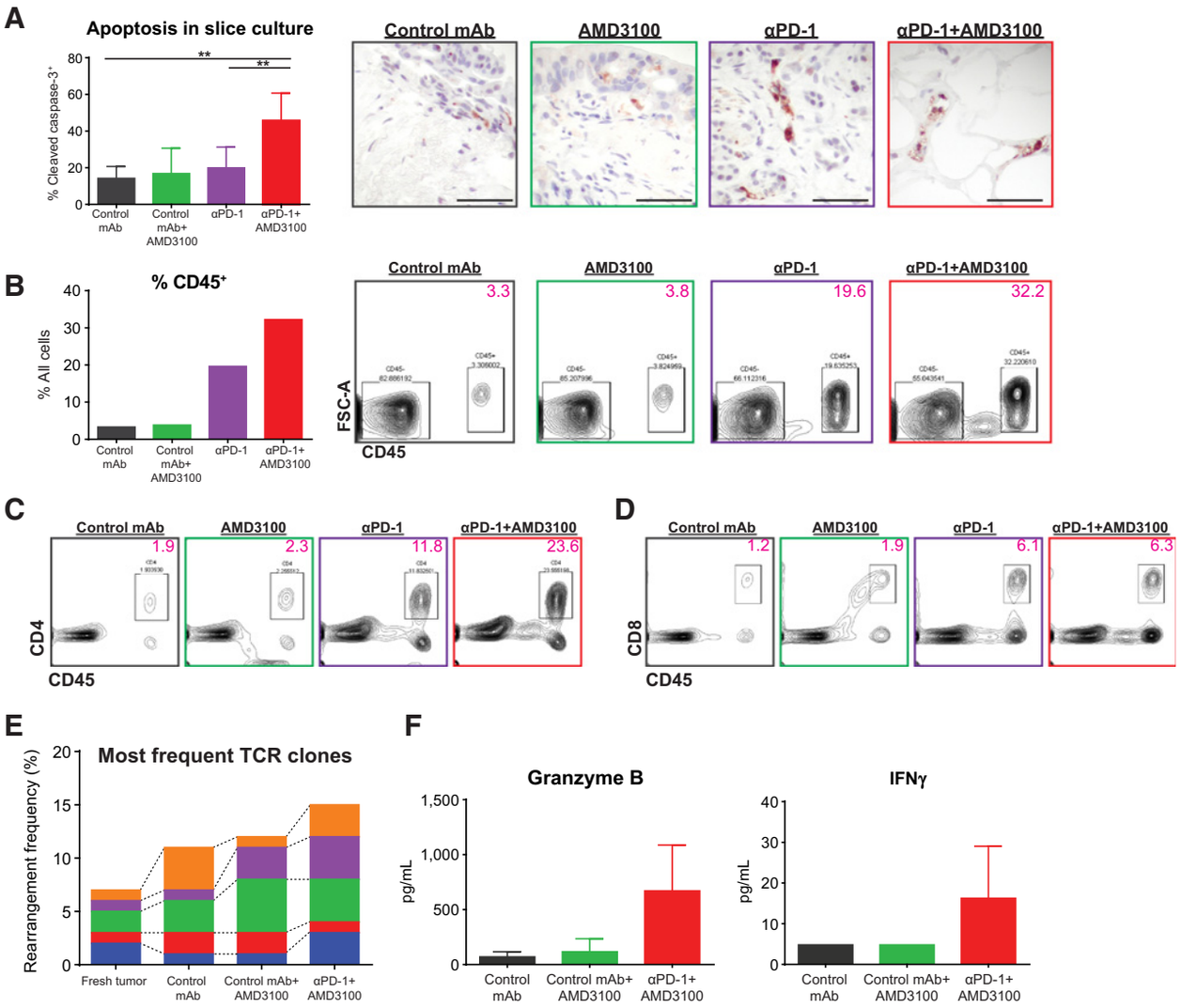

Figure 4.

Tumor killing with combination immunotherapy is mediated by T-cell activity. **A,** Percent of all cells per high-powered field positive for cleaved Caspase-3 on IHC. Unpaired Student *t* tests; **, $P < 0.01$. Representative images after treatment for 6 days *in vitro* (scale bars, 50 μm). Experiment repeated in 3 patients showing similar results. **B–D,** Representative flow cytometric analysis of disaggregated tumor slices after 2 days of treatment *in vitro*. Immune cell percentage increased with combination immunotherapy, driven mostly by both $CD4^+$ and $CD8^+$ T cells. Data representative of 3 total experiments. TCR sequencing and cytokine quantification of supernatant from slices from the same tumor treated for 2 days. **E,** Each bar represents a TCR clone present across slices in different treatment groups. **F,** Supernatant was tested for presence of granzyme B and IFNγ after 2 days in culture.

(Fig. 4A; Supplementary Fig. S4A and S4B). Flow cytometry of disaggregated tumor slices demonstrated increased frequency of $CD45^+$ immune cells, including both $CD4^+$ and $CD8^+$ cells, following either combination or anti-PD-1 therapy (Fig. 4B–D; Supplementary Fig. S4C).

Given the nature of the tumor slice culture model, which focuses on *in situ* intratumoral T cells, we predicted that this increased T-cell frequency represented activation and expansion of resident tumor-specific clones. To test this hypothesis, we performed TCR immunosequencing on tumor slices after treatment *ex vivo*. Importantly, we demonstrated preservation of high-frequency clones, with further expansion of selected clones following combination therapy (Fig. 4E). Supernatant from cultures demonstrated analogous increases in effector molecules, such as granzyme B and IFNγ, reflecting T-cell activation concurrent with proliferation and clonal expansion (Fig. 4F). These results suggested that combination therapy enhanced tumor cell killing through reactivation of tumor antigen–specific intratumoral $CD8^+$ T-cell clones.

Tumor cell death from combined PD-1 and CXCR4 blockade is a result of enhanced $CD8^+$ T-cell migration and cytotoxicity

To assess whether the enhanced antitumor effect of combined PD-1 and CXCR4 blockade depended on T-cell–mediated killing, we performed time-lapse confocal microscopy of live PDA slice cultures, which enabled real-time visualization of $CD8^+$ T cell and

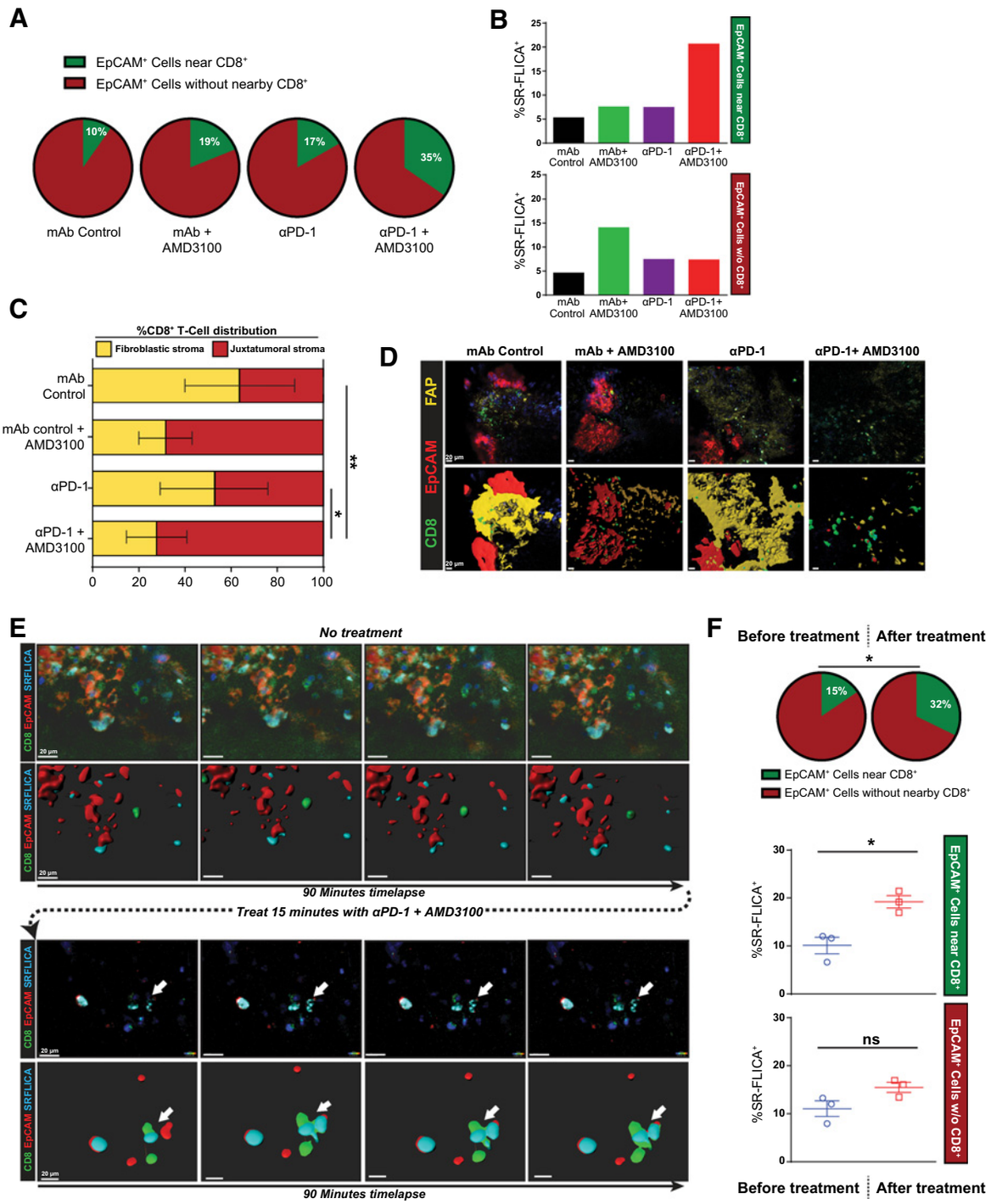

Figure 5.

Mobilization of CD8$^+$ T cells into juxtatumoral areas via CXCR4 blockade facilitates PD-1 inhibition–mediated tumor cell killing. Compiled data of live tumor imaging of multiple tumors after 2 days of treatment *in vitro* ($n = 3$). **A,** Percent of tumor cells (EpCAM$^+$) within 20 μm of at least 1 CD8$^+$ T cell (green pie) after *in vitro* treatment in slice culture. **B,** SR-FLICA positivity denotes activated cleaved Caspase-3 and -7. **C** and **D,** CD8$^+$ T-cell infiltration in fibroblastic stroma versus juxtatumoral areas after 2 days of treatment ($n = 3$), and representative images showing fibroblast-activated protein (FAP) staining in yellow. Representative single slice time-lapse imaging before and after combination treatment ($n = 3$). **E,** Time-lapse images showing the same live tumor slice with no treatment, followed by incubation with combination immunotherapy and subsequent time-lapse. Arrow points to dynamic CD8-tumor cell interaction leading to SR-FLICA staining. **F,** Percent of tumor cells near CD8$^+$ T cell before and after treatment (green pie). %SR-FLICA$^+$ increases in tumor cells near CD8$^+$ T cells, but not in those more than 20 μm of CD8$^+$ T cell ($n = 3$; paired Student *t* test, *, $P < 0.05$; **, $P < 0.01$; error bars, SEM).

$EpCAM^+$ tumor cell interactions. Combined PD-1 and CXCR4 blockade increased the number of $EpCAM^+$ cells surrounded by $CD8^+$ T cells after 2 days, compared with monotherapy or negative control (Fig. 5A and B; Supplementary Fig. S5A). Furthermore, tumor cell apoptosis, as evidenced by SR-FLICA fluorescent labeling of activated Caspase-3 and -7 enzymes, was disproportionately increased in $EpCAM^+$ cells abutting $CD8^+$ T cells. This phenomenon was only seen after combined PD-1 and CXCR4 blockade, and not with either monotherapy or control (Fig. 5A and B; Supplementary Fig. S5A). Concurrently, combination treatment shifted the distribution of $CD8^+$ T cells from the fibroblastic stroma into the immediate juxtatumoral stroma containing $EpCAM^+$ cells (Fig. 5C and D; Supplementary Fig. S5B).

To confirm that these findings do not simply represent homing of $CD8^+$ T cells toward tumor cells dying from direct cytotoxic activity of the drugs, we assessed the short-term effects of combined PD-1 and CXCR4 blockade. Indeed, time-lapse fluorescent imaging of treated slice cultures depicted a striking redistribution and activation of T-cell–mediated killing in real-time. At baseline, PDA slices demonstrated only a low level of SR-FLICA positivity among $EPCAM^+$ cells. However, within 2 hours of adding PD-1 and CXCR4 blocking agents, we detected a similar increase in $EpCAM^+$ cells with a $CD8^+$ T cell in close proximity, as well as increased apoptosis in these specific tumor cells (Fig. 5E and F; Supplementary Fig. S5C). The total proportion of $EpCAM^+$ carcinoma cells which were undergoing apoptosis was increased compared with IgG isotype control, additionally suggesting that the increased epithelial cell apoptosis was dependent on cytotoxic T-cell proximity (Supplementary Fig. S5C). Importantly, a similar short-term time-lapse experiment in which the cultures were treated with a control mAb showed no changes in $CD8^+$ T-cell migration or cytotoxic activity. (Supplementary Fig. S5D). These results demonstrate the ability of combined PD-1 and CXCR4 blockade to rapidly alter intratumoral T-cell migration and activation thresholds, ultimately unleashing the direct cytotoxic effects of activated resident $CD8^+$ T cells on tumor cells within human PDA.

Discussion

The promise of successful immunotherapy remains an elusive goal for patients with PDA. Mouse models of PDA suggest that fibrosis around the cancer cells and immunosuppressive elements such as myeloid-derived suppressor prevent T_{eff} infiltration and activation; therefore, this is often cited as the root cause of the lack of clinical response to immunotherapy (36–39). By overcoming different aspects of this putatively immunosuppressive environment, groups have been able to make murine models of PDA more sensitive to immunotherapy (36, 37). In contrast to these mouse models, human PDA has been shown to have a robust T-cell infiltration, and the degree of infiltration into the peritumoral area has been correlated with improved clinical outcomes (11, 12, 40). Our current immunophenotypic data on human PDA shows less infiltration of $CD8^+$ T cells along with greater infiltration of immunosuppressive Treg phenotypes in juxtatumoral areas. In the setting of such an immune-excluded tumor microenvironment, using 2 clinically active immunotherapy agents, a CXCR4 inhibitor and a PD-1–blocking antibody, we have herein demonstrated the first direct evidence of T-cell–mediated tumor killing in PDA.

The presence of clonally expanded T cells in PDA has recently been demonstrated (27, 28). Using a larger number of patient tumors and evaluating multiple regions of a subset of the tumors, we found that there was conservation of dominant clones across a wide geographic area (2 different blocks from the same tumor). Maintenance of dominant T-cell clones was even evident in 1 patient, who had 2 anatomically distinct, synchronous primary tumors, which demonstrated considerable clonal overlap. Furthermore, we found multiple T-cell receptor DNA rearrangements coding for the same high frequency, presumably high-affinity amino acid sequences, suggesting positive selection of a tumor-specific T-cell response to PDA. This evidence of clonal evolution of TCRs in a tumor has not, to our knowledge, been previously reported and is the subject of ongoing study. Future work will include single-cell sequencing of both the alpha and beta chains of the TCR variable region to determine the true overlap in antigen specificity of these dominant clones. In-depth TCR profiling will additionally serve as the foundation for identifying putative tumor-specific antigens underlying this adaptive antitumor response.

Our finding that potentially antitumor $PD\text{-}1^+CD8^+$ T cells tended to localize to the stromal regions lacking carcinoma cells and that clonality was inversely related to Treg infiltration suggested that reactivation of preexisting, tumor-specific resident T cells in human tumors might require alteration of T-cell migration, in addition to standard immune checkpoint inhibition. We therefore tested CXCR4 blockade in combination with PD-1/PD-L1 blockade, as it was shown by Feig and colleagues to activate antitumor immunity in a murine PDA model system (24); however, the mechanism of activity of this combination had not been fully elucidated, nor had its effects in human tumors been demonstrated. Indeed, we found a synergistic increase in tumor cell apoptosis, concomitant with *ex vivo* expansion and activation of T cells localized to the same area of tumor. Our findings are all the more striking because of the consistency with which combined PD-1 and CXCR4 blockade enhances $CD8^+$ T-cell–mediated antitumor activity in numerous different patients' tumors. This speaks to the potentially broad clinical applicability of this therapy despite genotypic and phenotypic heterogeneity among different patients and tumors.

We confirmed the role of $CD8^+$ T cells in this enhanced response to combination therapy through the novel application of live fluorescent microscopy of the tumor slice culture platform. While others have performed similar techniques in lung and ovarian cancer slice culture models to demonstrate T-cell migration (41–43), we present a novel use of this technology to precisely track both $CD8^+$ T-cell migration and antitumor activity within the tumor microenvironment. Using this platform in separate tumor slices undergoing various treatments, as well as individual slices treated over time, we were able to provide direct evidence that combined PD-1 and CXCR4 blockade activates $CD8^+$ T cells within the human PDA microenvironment to migrate to and kill tumor cells. We found redistribution of $CD8^+$ T cells from the fibroblastic to juxtatumoral stroma after CXCR4 blockade alone, while increased apoptosis of $EpCAM^+$ cells was noted only with combination treatment, suggesting improved chemotaxis is insufficient to activate tumor cell killing. Furthermore, the speed with which combination treatment increased both tumor cell-to-$CD8^+$ T-cell proximity and tumor cell apoptosis, an effect seen within 2 hours of drug exposure in live slice culture, confirms reactivation of preexisting T-cell clones. Future studies will further dissect the in-depth mechanisms of synergism

between PD-1 and CXCR4 axes blockade in overcoming the pathogenic effects of immune exclusion.

Our data thus argue against the currently accepted paradigm that the reason immunotherapy does not work in human PDA is a lack of immunogenicity or generation of tumor-specific T-cell responses (44, 45). Rather, it is due to sequestration of already, clonally expanded tumor-reactive T cells away from the juxtatumoral compartment, which can be reversed by targeting the CXCL12/CXCR4 pathway. Given that, it is believed that human PDA undergoes a prolonged evolution (46, 47), we postulate that the adaptive immune response to PDA coevolves with the tumor through the dynamic process of immunoediting. In the context of this complex tumor microenvironment, effective immunotherapy against PDA and other tumors demonstrating immune exclusion will require modulation of multiple axes of immunosuppression, including addressing the problem of geographic sequestration of T_{eff}.

Disclosure of Potential Conflicts of Interest

S. M. Pollack reports receiving commercial research grants from Merck, EMD Serono, and Incyte. R. H. Pierce reports receiving commercial research grants from X4 Pharma. H. Robins is an employee of and holds ownership interest (including patents) in Adaptive Biotechnologies. V.G. Pillarisetty reports receiving commercial research grants from and is a consultant/advisory board member for Merck Sharp & Dohme Corp. No potential conflicts of interest were disclosed by the other authors.

Authors' Contributions

Conception and design: Y.D. Seo, R.H. Pierce, V.G. Pillarisetty
Development of methodology: Y.D. Seo, K.M. Sullivan, K.S. Smythe, R.H. Pierce, H. Robins, V.G. Pillarisetty, X. Jiang
Acquisition of data (provided animals, acquired and managed patients, provided facilities, etc.): K.M. Sullivan, K.S. Smythe, A. Abbasi, J.O. Park, V.G. Pillarisetty, X. Jiang
Analysis and interpretation of data (e.g., statistical analysis, biostatistics, computational analysis): Y.D. Seo, K.M. Sullivan, F.G. Jalikis, M. Vignali, S.K. Daniel, S.M. Pollack, T.S. Kim, R.H. Pierce, H. Robins, V.G. Pillarisetty, X. Jiang
Writing, review, and/or revision of the manuscript: Y.D. Seo, K.M. Sullivan, F.G. Jalikis, K.S. Smythe, M. Vignali, J.O. Park, S.K. Daniel, S.M. Pollack, T.S. Kim, R. Yeung, I.N. Crispe, R.H. Pierce, V.G. Pillarisetty, X. Jiang
Administrative, technical, or material support (i.e., reporting or organizing data, constructing databases): Y.D. Seo, K.S. Smythe, V.G. Pillarisetty
Study supervision: Y.D. Seo, V.G. Pillarisetty

Acknowledgments

We thank Allison Leahy for consenting patients for research tissue collection. We acknowledge support from the NIH (S10 OD016240) to the W.M. Keck Center for Advanced Studies in Neural Signaling and the assistance of Keck Center manager Dr. Nathaniel Peters. We also acknowledge the Fred Hutchinson Cancer Research Center Cores for flow cytometry and for experimental histopathology in providing critical support for our experimentation. V.G. Pillarisetty was supported by Parvin Valentini Fund for Pancreatic Cancer Research, Donald E. Bocek Endowed Research Development Award in Pancreatic Cancer, United States Army Medical Research Acquisition Activity (USAMRAA; CA150370P2), Swim Across America, and Merck Investigator Studies Program. Y.D. Seo was supported by Swim Across America. I.N. Crispe was supported by the Seattle Foundation.

The costs of publication of this article were defrayed in part by the payment of page charges. This article must therefore be hereby marked *advertisement* in accordance with 18 U.S.C. Section 1734 solely to indicate this fact.

Received January 8, 2019; revised March 25, 2019; accepted March 27, 2019; published first April 2, 2019.

References

1. Siegel RL, Miller KD, Jemal A. Cancer statistics, 2018. CA Cancer J Clin 2018;68:7–30.
2. Ribas A, Hamid O, Daud A, Hodi FS, Wolchok JD, Kefford R, et al. Association of pembrolizumab with tumor response and survival among patients with advanced melanoma. JAMA 2016;315:1600–9.
3. Brahmer JR, Tykodi SS, Chow LQM, Hwu W-J, Topalian SL, Hwu P, et al. Safety and activity of anti-PD-L1 antibody in patients with advanced cancer. N Engl J Med 2012;366:2455–65.
4. Royal RE, Levy C, Turner K, Mathur A, Hughes M, Kammula US, et al. Phase 2 trial of single agent Ipilimumab (anti-CTLA-4) for locally advanced or metastatic pancreatic adenocarcinoma. J Immunother 2010;33:828–33.
5. Clark CE, Beatty GL, Vonderheide RH. Immunosurveillance of pancreatic adenocarcinoma: insights from genetically engineered mouse models of cancer. Cancer Lett 2009;279:1–7.
6. Bayne LJ, Beatty GL, Jhala N, Clark CE, Rhim AD, Stanger BZ, et al. Tumor-derived granulocyte-macrophage colony-stimulating factor regulates myeloid inflammation and T cell immunity in pancreatic cancer. Cancer Cell 2012;21:822–35.
7. Beatty GL, Chiorean EG, Fishman MP, Saboury B, Teitelbaum UR, Sun W, et al. CD40 agonists alter tumor stroma and show efficacy against pancreatic carcinoma in mice and humans. Science 2011;331:1612–6.
8. Chen DS, Mellman I. Elements of cancer immunity and the cancer–immune set point. Nature 2017;541:321–30.
9. Fukunaga A, Miyamoto M, Cho Y, Murakami S, Kawarada Y, Oshikiri T, et al. CD8+ tumor-infiltrating lymphocytes together with CD4+ tumor-infiltrating lymphocytes and dendritic cells improve the prognosis of patients with pancreatic adenocarcinoma. Pancreas 2004;28:e26–31.
10. Ino Y, Yamazaki-Itoh R, Shimada K, Iwasaki M, Kosuge T, Kanai Y, et al. Immune cell infiltration as an indicator of the immune microenvironment of pancreatic cancer. Br J Cancer 2013;108:914–23.
11. Shibuya KC, Goel VK, Xiong W, Sham JG, Pollack SM, Leahy AM, et al. Pancreatic ductal adenocarcinoma contains an effector and regulatory immune cell infiltrate that is altered by multimodal neoadjuvant treatment. PLoS One 2014;9:e96565.
12. Carstens JL, Correa de Sampaio P, Yang D, Barua S, Wang H, Rao A, et al. Spatial computation of intratumoral T cells correlates with survival of patients with pancreatic cancer. Nat Commun 2017;8:15095.
13. Bauer C, Kühnemuth B, Duewell P, Ormanns S, Gress T, Schnurr M. Prevailing over T cell exhaustion: new developments in the immunotherapy of pancreatic cancer. Cancer Lett 2016;381:259–68.
14. Caruz A, Samsom M, Alonso JM, Alcami J, Baleux F, Virelizier JL, et al. Genomic organization and promoter characterization of human CXCR4 gene 1. FEBS Lett 426:271–8.
15. Moriuchi M, Moriuchi H, Turner W, Fauci AS. Cloning and analysis of the promoter region of CXCR4, a coreceptor for HIV-1 entry. J Immunol 1997;159:4322–9.
16. Wegner SA, Ehrenberg PK, Chang G, Dayhoff DE, Sleeker AL, Michael NL. Genomic organization and functional characterization of the chemokine receptor CXCR4, a major entry co-receptor for human immunodeficiency virus type 1. J Biol Chem 1998;273:4754–60.
17. Kalatskaya I, Berchiche YA, Gravel S, Limberg BJ, Rosenbaum JS, Heveker N. AMD3100 is a CXCR7 ligand with allosteric agonist properties. Mol Pharmacol 2009;75:1240–7.
18. Liu Q, Li Z, Gao J-L, Wan W, Ganesan S, McDermott DH, et al. CXCR4 antagonist AMD3100 redistributes leukocytes from primary immune organs to secondary immune organs, lung, and blood in mice. Eur J Immunol 2015;45:1855–67.
19. Wagstaff AJ. Plerixafor: in patients with non-Hodgkin's lymphoma or multiple myeloma. Drugs 2009;69:319–26.
20. Mirisola V, Zuccarino A, Bachmeier BE, Sormani MP, Falter J, Nerlich A, et al. CXCL12/SDF1 expression by breast cancers is an independent

prognostic marker of disease-free and overall survival. Eur J Cancer 2009; 45:2579–87.
21. Sun X, Cheng G, Hao M, Zheng J, Zhou X, Zhang J, et al. CXCL12/CXCR4/CXCR7 chemokine axis and cancer progression. Cancer Metastasis Rev 2010;29:709–22.
22. Gil M, Komorowski MP, Seshadri M, Rokita H, McGray AJR, Opyrchal M, et al. CXCL12/CXCR4 blockade by oncolytic virotherapy inhibits ovarian cancer growth by decreasing immunosuppression and targeting cancer-initiating cells. J Immunol 2014;193:5327–37.
23. Chen Y, Ramjiawan RR, Reiberger T, Ng MR, Hato T, Huang Y, et al. CXCR4 inhibition in tumor microenvironment facilitates anti-programmed death receptor-1 immunotherapy in sorafenib-treated hepatocellular carcinoma in mice. Hepatology 2015;61:1591–602.
24. Feig C, Jones JO, Kraman M, Wells RJB, Deonarine A, Chan DS, et al. Targeting CXCL12 from FAP-expressing carcinoma-associated fibroblasts synergizes with anti-PD-L1 immunotherapy in pancreatic cancer. Proc Natl Acad Sci U S A 2013;110:20212–7.
25. Kirsch I, Vignali M, Robins H. T-cell receptor profiling in cancer. Mol Oncol 2015;9:2063–70.
26. Reuben A, Gittelman R, Gao J, Zhang J, Yusko EC, Wu C-J, et al. TCR repertoire intratumor heterogeneity in localized lung adenocarcinomas: an association with predicted neoantigen heterogeneity and postsurgical recurrence. Cancer Discov 2017;7:1088–97.
27. Stromnes IM, Hulbert A, Pierce RH, Greenberg PD, Hingorani SR. T-cell localization, activation, and clonal expansion in human pancreatic ductal adenocarcinoma. Cancer Immunol Res 2017;5:978–91.
28. Poschke I, Faryna M, Bergmann F, Flossdorf M, Lauenstein C, Hermes J, et al. Identification of a tumor-reactive T-cell repertoire in the immune infiltrate of patients with resectable pancreatic ductal adenocarcinoma. Oncoimmunology 2016;5:e1240859.
29. Balachandran VP, èuksza M, Zhao JN, Makarov V, Moral JA, Remark R, et al. Identification of unique neoantigen qualities in long-term survivors of pancreatic cancer. Nature 2017;551:512–6.
30. Jiang X, Seo YD, Chang JH, Coveler A, Nigjeh EN, Pan S, et al. Long-lived pancreatic ductal adenocarcinoma slice cultures enable precise study of the immune microenvironment. Oncoimmunology 2017;6:e1333210.
31. Jiang X, Seo YD, Sullivan KM, Pillarisetty VG. Establishment of slice cultures as a tool to study the cancer immune microenvironment. In: López-Soto A, Folgueras AR, editors. Cancer immunosurveillance: methods and protocols. New York, NY: Springer New York; 2019. p. 283–95.
32. Carlson CS, Emerson RO, Sherwood AM, Desmarais C, Chung M-W, Parsons JM, et al. Using synthetic templates to design an unbiased multiplex PCR assay. Nat Commun 2013;4:2680.
33. Jiang Y, Du Z, Yang F, Di Y, Li J, Zhou Z, et al. FOXP3+ lymphocyte density in pancreatic cancer correlates with lymph node metastasis. PLoS One 2014;9:e106741.
34. Allison KH, Sledge GW. Heterogeneity and cancer. Oncology 2014;28: 772–8.
35. Cai W, Lin D, Wu C, Li X, Zhao C, Zheng L, et al. Intratumoral heterogeneity of ALK-rearranged and ALK/EGFR coaltered lung adenocarcinoma. J Clin Oncol 2015;33:3701–9.
36. Zhu Y, Knolhoff BL, Meyer MA, Nywening TM, West BL, Luo J, et al. CSF1/CSF1R blockade reprograms tumor-infiltrating macrophages and improves response to T-cell checkpoint immunotherapy in pancreatic cancer models. Cancer Res 2014;74:5057–69.
37. Jiang H, Hegde S, Knolhoff BL, Zhu Y, Herndon JM, Meyer MA, et al. Targeting focal adhesion kinase renders pancreatic cancers responsive to checkpoint immunotherapy. Nat Med 2016;22:851–60.
38. Panni RZ, Linehan DC, DeNardo DG. Targeting tumor-infiltrating macrophages to combat cancer. Immunotherapy 2013;5:1075–87.
39. Goedegebuure P, Mitchem JB, Porembka MR, Tan MCB, Belt BA, Wang-Gillam A, et al. Myeloid-derived suppressor cells: general characteristics and relevance to clinical management of pancreatic cancer. Curr Cancer Drug Targets 2011;11:734–51.
40. Ene-Obong A, Clear AJ, Watt J, Wang J, Fatah R, Riches JC, et al. Activated pancreatic stellate cells sequester CD8+ T cells to reduce their infiltration of the juxtatumoral compartment of pancreatic ductal adenocarcinoma. Gastroenterology 2013;145:1121–32.
41. Salmon H, Franciszkiewicz K, Damotte D, Dieu-Nosjean M-C, Validire P, Trautmann A, et al. Matrix architecture defines the preferential localization and migration of T cells into the stroma of human lung tumors. J Clin Invest 2012;122:899–910.
42. Salmon H, Rivas-Caicedo A, Asperti-Boursin F, Lebugle C, Bourdoncle P, Donnadieu E. *Ex vivo* imaging of T cells in murine lymph node slices with widefield and confocal microscopes. J Vis Exp 2011;53:e3054, doi: 10.3791/3054.
43. Bougherara H, Mansuet-Lupo A, Alifano M, Ngô C, Damotte D, Le Frère-Belda M-A, et al. Real-time imaging of resident T cells in human lung and ovarian carcinomas reveals how different tumor microenvironments control T lymphocyte migration. Front Immunol 2015;6:500.
44. Vonderheide RH. The immune revolution: a case for priming, not checkpoint. Cancer Cell 2018;33:563–9.
45. Winograd R, Byrne KT, Evans RA, Odorizzi PM, Meyer ARL, Bajor DL, et al. Induction of T-cell immunity overcomes complete resistance to PD-1 and CTLA-4 blockade and improves survival in pancreatic carcinoma. Cancer Immunol Res 2015;3:399–411.
46. Iacobuzio-Donahue CA. Genetic evolution of pancreatic cancer: lessons learnt from the pancreatic cancer genome sequencing project. Gut 2012;61: 1085–94.
47. Martinez-Bosch N, Vinaixa J, Navarro P. Immune evasion in pancreatic cancer: from mechanisms to therapy. Cancers 2018;10:6.